Ductile End-Diaphragms for Seismic Retrofit of Slab-on-Girder Steel Bridges

By Seyed Mehdi Zahrai[1] and Michel Bruneau,[2] Member, ASCE

ABSTRACT: Steel bridges are frequently supported by seismically vulnerable substructures, as clearly demonstrated by recent earthquakes. The seismic retrofit of these nonductile substructures can be, in many cases, a rather costly operation. This paper investigates the adequacy of a seismic retrofit strategy that relies instead on ductile end-diaphragms inserted in the steel superstructure: the objective is to protect the substructure by replacing the steel diaphragms over abutments and piers with specially designed ductile diaphragms calibrated to yield before the strength of the substructure is reached. For a type of steel slab-on-girder bridge widely found in North America, this paper presents simplified analytical models as well as a step-by-step design procedure developed for three types of ductile diaphragm systems (such as shear panels, eccentrically braced frames, and triangular-plate added damping and stiffness devices), followed by results from nonlinear inelastic analyses conducted to investigate the seismic behavior of these retrofitted bridges. At this time, only bridges on stiff substructure are considered, although a few examples are presented to illustrate the potential inadequacy of this retrofit approach for bridges on flexible substructures.

INTRODUCTION

The recent Northridge and Kobe earthquakes (among many) clearly demonstrated the seismic vulnerability of steel bridges supported by nonductile substructure elements. Although damage to superstructure components of these bridges is also possible, mostly in the form of buckling and/or connection fracture of diaphragm braces, damage to substructure components such as abutments, piers, and bearings, have proven to be of far greater consequence, often leading to span collapses (Roberts 1992; Astaneh-Asl et al. 1994; Bruneau et al. 1996).

Hence, when existing bridges are targeted for seismic rehabilitation, much attention is paid to these substructure elements. Typically, the current retrofitting practice is to either strengthen or replace the existing nonductile members (e.g., Seismic 1983; Buckle et al. 1986; ''Bridge'' 1993; Shirolé and Malik 1993), enhance their ductility capacity (e.g., Degenkolb 1978; Priestly et al. 1992), or reduce the force demands on the vulnerable substructure elements using base isolation techniques or other structural modifications (e.g., Mayes et al. 1992; Astaneh-Asl 1993). Whereas all these approaches are proven effective solutions, only the base isolation concept currently recognizes that seismic deficiency attributable to substructure weaknesses may be resolved by operating elsewhere than on the substructure itself. Moreover, all approaches can be costly, even base isolation in those instances when significant abutment modifications and other structural changes are needed to permit large displacements at the isolation bearings and lateral load redistribution among piers (Mayes et al. 1994).

A seismic retrofit strategy that relies instead on ductile end-diaphragms inserted in the steel superstructure, if effective, could provide an interesting alternative. In some cases, by replacing the steel diaphragms over abutments and piers with specially designed ductile diaphragms calibrated to yield before the strength of the substructure is reached, damage can be prevented from developing in the nonductile substructural

elements, foundation, and bearings (hereafter referred to generically as ''substructure''). This objective is schematically illustrated in Fig. 1. Many types of systems capable of stable passive seismic energy dissipation could be used for this purpose. Among those, eccentrically braced frames (EBF) (e.g., Malley and Popov 1983; Kasai and Popov 1986), shear panel systems (SPS) (Fehling et al. 1992; Nakashima 1995), and steel triangular-plate added damping and stiffness devices (TADAS) (Tsai et al. 1993) have received particular attention in building applications. Still, to the writers' knowledge, to date none of these applications has been considered for bridge structures. This may be partly attributable to the absence of seismic ductile steel detailing provisions in North American bridge codes. Examples of how these systems would be implemented in the end-diaphragms of a typical 40 m span bridge are shown in Figs. 2(a–c). Note that although concentrically braced frames can also be ductile, they are not considered here because they often are stronger than calculated and their hysteretic curves can exhibit pinching and some strength degradation.

The objective of this paper is to investigate the adequacy of this ductile end-diaphragm rehabilitation concept for a type of steel slab-on-girder bridge widely found in North America. Simplified analytical models, as well as step-by-step design procedures developed for three types of ductile diaphragm systems (SPS, EBF, and TADAS devices), are first presented, followed by results from nonlinear inelastic analyses conducted to investigate the seismic behavior of these retrofitted bridges.

At this time, only bridges on stiff substructure are considered, although a few examples are presented to illustrate the potential inadequacy of this retrofit approach for bridges on

[1]Postdoctoral Fellow, Build. Perf. Lab., M24 Build., Nat. Res. Council Canada, 1500 Montreal Rd., Pasteur, Ottawa, ON, Canada K1A 0R6. E-mail: seyed.zahrai@nrc.ca

[2]Prof., Dept. of Civ., Struct., and Envir. Engrg., 130 Ketter Hall, State Univ. of New York at Buffalo, Buffalo, NY 14260. E-mail: bruneau@acsu.buffalo.edu
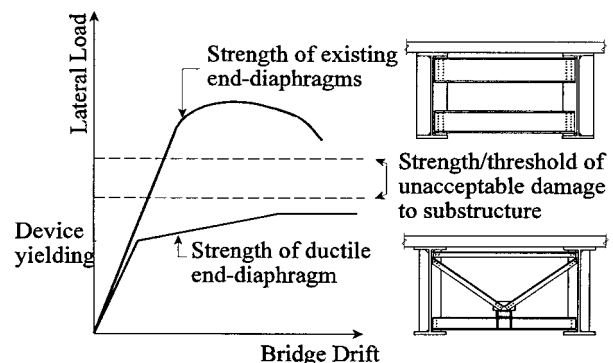
FIG. 1. Inelastic Behavior of Ductile End-Diaphragms Compared with Existing Strong Diaphragms
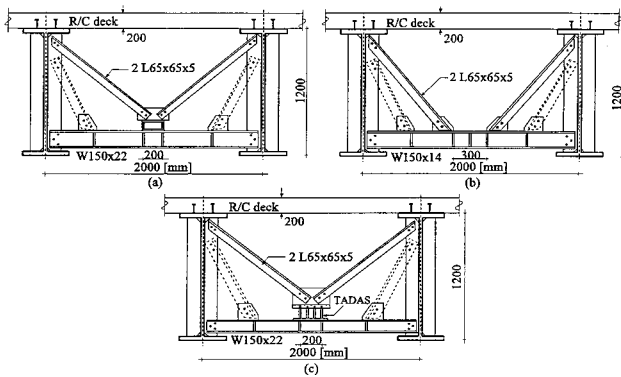
FIG. 2. Ductile End-Diaphragms of Typical 40 m Span Bridge: (a) SPS; (b) EBF; (c) TADAS (Other Unbraced Girders Not Shown; Dotted Members only if Required for Jacking Purposes for Nonseismic Reasons)

FIG. 3. Proposed Simplified 2D Model of End-Diaphragm: (a) 3D View of Ductile System (Deck Not Shown); (b) Spring Modeling of Typical Bridge in Transverse Direction, also Showing Generalized Mass and Stiffness for One Bridge End; (c) Simple Spring Model of Dual System

flexible substructures. The scope of this study is also limited to bridges that do not have horizontal wind bracing connecting the bottom flanges of girders, because these braces could provide an alternative load path bypassing the special ductile elements. Note that this retrofit method only provides enhanced seismic resistance and substructure protection for the component of seismic excitation transverse to the bridge and must be coupled with other devices that constrain longitudinal seismic displacements, such as simple bearings strengthening (Mander et al. 1996) and rubber bumpers; transportation agencies experienced in seismic bridge retrofit have indicated that deficiencies in the longitudinal direction of these bridges are typically easier to address than those in the lateral direction (Brock Radloff, Ministry of Transportation of British Columbia, private communication).

ANALYTICAL DEVELOPMENT

Formulation of Two-Dimensional (2D) Model

To provide computational efficiency and to allow formulation of a simple design procedure (presented in a later section), a simplified 2D model capturing the essence of the three-dimensional (3D) behavior of slab-on-girder bridges was developed. The availability of a 2D model was also appealing because it made possible the use of DRAIN-2DX for the subsequent studies of seismic nonlinear behavior. The proposed simplified 2D model is a ''stick'' model of the structural assembly shown in Fig. 3(a). It consists of the ductile end-diaphragm, a stub-length of two girders with their bearing stiffeners, a rigid stub of the reinforced concrete deck, and a small mass/spring subsystem located at deck level and introduced to account for the longitudinal generalized mass and stiffness effects. It is noteworthy that bearing web stiffeners provide the main stiffness for girders; in other words, using a longer length of girders in the stub-girder model results in no significant difference in model stiffness, as demonstrated later.

The generalized mass, m^*, stiffness, K^*, and effective force, P_{eff}, for a simply supported bridge superstructure model can be calculated assuming that the first transverse mode shape of the superstructure between supports can be represented by the following sine shape function:

$$u(x) = \sin \frac{\pi x}{L} \tag{1}$$

where L = span length. Therefore, ignoring deck displacements at the bridge ends

$$m^* = \int_0^L \frac{M}{L} (u(x))^2 \, dx = \frac{M}{2} \tag{2a}$$
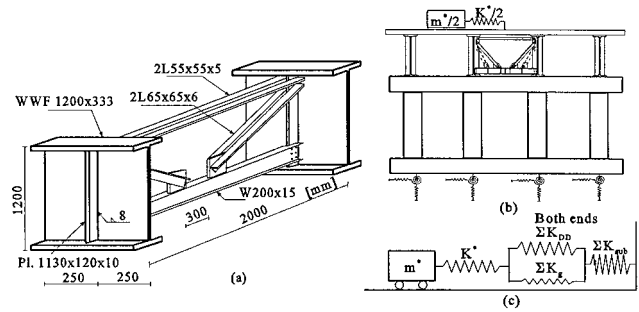
$$K^* = \int_0^L EI_D \left(\frac{d^2u(x)}{dx^2}\right)^2 dx = \frac{\pi^4 EI_D}{2L^3} \tag{2b}$$

and

$$P_{eff} = PSa \int_0^L \frac{M}{L} u(x); \quad dx = \frac{2M}{\pi} PSa = \frac{4m^*}{\pi} PSa \tag{3}$$

where M = mass of the entire bridge; E = modulus of elasticity; I_D = moment of inertia of the whole superstructure section (i.e., concrete deck and steel girders transformed section) about a vertical axis perpendicular to the deck; and PSa is the design pseudo acceleration.

While the above 2D model can be implemented directly for computer analyses, its simplicity makes it also suitable for hand calculations. Indeed, recognizing that the generalized stiffness of the bridge superstructure, K^*, the lateral stiffness of the end-diaphragms, K_{ends}, and the lateral stiffness of substructure including abutments, columns, piers, foundations, and soils, K_{subs}, are linked together as springs in series [Figs. 3(b and c)], the equivalent stiffness of the entire bridge, K_e, can be written as:

$$K_e = \frac{1}{\dfrac{1}{K^*} + \dfrac{1}{K_{ends}} + \dfrac{1}{K_{subs}}} \tag{4}$$

For the single-span bridges supported on stiff substructures considered here, the substructure flexibility term is ignored. Note that the plate girders can potentially contribute to the lateral load resistance, making the end-diaphragm behave as a dual system, as shown in Fig. 3(c) (two springs in parallel). Therefore, the lateral stiffness of the stiffened girders, ΣK_g, must be added to the stiffness of the ductile diaphragms, ΣK_{DD} (usually much larger than the former), to obtain the lateral stiffness of the bridge end-diaphragms (adding the stiffnesses of both ends of the span), K_{ends}, i.e.

$$K_{ends} = \sum K_{DD} + \sum K_g \tag{5}$$

The stiffness contribution of a plate girder is obviously a function of the fixity provided to its top and bottom flanges by the deck slab and bearing, respectively. If full fixity is provided at both flanges of the plate girder

$$K_g = \frac{12EI_g}{h_g^3} \tag{6}$$

where I_g = moment of inertia of the stiffened stub girder (mainly due to the bearing web stiffeners) in the lateral direction; and h_g = its height. If one end is fully fixed, the other one pinned

$$K_g = \frac{3EI_g}{h_g^3} \quad (7)$$

If both ends effectively behave as pin supports, $K_g = 0$. The actual amount of fixity provided can be difficult to accurately estimate. Full fixity at the deck level in composite bridges is possible if the shear studs originally installed to allow this composite action are closely spaced and can resist the pull-out forces resulting from the moments developed at the top of the girders under lateral seismic forces. As for fixity at the bearing level, it obviously depends on the type of bearings present. However, even when infinitely rigid bearings are present, full fixity is still difficult to ensure due to flexibility of the girder flanges, as revealed by finite-element analyses of subassemblies at the girder-to-bearing connection point.

It is obviously the engineer's responsibility to determine the level of fixity provided at the ends of the girders. However, contrary to conventional design, the most conservative solution is not obtained when zero fixity is assumed because fixity also adds strength to the diaphragms, and the role of the ductile diaphragms is to limit the magnitude of the maximum forces that can develop in the substructure. In the examples reported in this paper, except where noted, a slightly conservative assumption was adopted by considering full fixity at the deck and zero fixity at the flexible bearings (rocking possibility). All other possible boundary conditions would simply be variations and/or simplifications from this case.

Finally, the lateral stiffness of the ductile diaphragms, K_{DD}, depends on the type of ductile device implemented. For example, if a ductile SPS is used, the stiffness of one such end-diaphragm in a slab-on-girder bridge, K_{SPS}, can be obtained by:

$$K_{SPS} = \frac{E}{\dfrac{l_b}{2A_b \cos^2\alpha} + \dfrac{L_s}{4A_{bb}} + \left(\dfrac{h_l^3}{3I_l} + \dfrac{2.6h_l}{A_{s,l}}\right) + \dfrac{L_s(h_l + d_{bb}/2)^2}{12I_{bb}} + \dfrac{H\tan^2\alpha}{2A_g}} \quad (8)$$

where E is the modulus of elasticity; l_b and A_b are the length and area of each brace; α is the brace's angle with the horizontal; L_s is the girder spacing; d_{bb}, A_{bb}, and I_{bb} are the depth, cross sectional area, and moment of inertia for the bottom beam; h_l, I_l, and $A_{s,l}$ are the length, moment of inertia, and shear area of the link; and H and A_g are the height and area of the stiffened girders.

Similarly, lateral stiffness of the EBF and TADAS implemented as end-diaphragms of slab-on-girder bridges, K_{EBF} and K_{TADAS}, can be computed as follows:

$$K_{EBF} = \frac{E}{\dfrac{l_b}{2A_b \cos^2\alpha} + \dfrac{a}{2A_l} + \dfrac{e^2H^2}{12L_sI_l} + \dfrac{1.3eH^2}{aL_sA_{s,l}} + \dfrac{H\tan^2\alpha}{2A_g}} \quad (9)$$

$$K_{TADAS} = \frac{E}{\dfrac{l_b}{2A_b \cos^2\alpha} + \dfrac{L_s}{4A_{bb}} + \dfrac{6h_T^3}{Nb_Tt_T^3} + \dfrac{L_s(h_T + d_{bb}/2)^2}{12I_{bb}} + \dfrac{H\tan^2\alpha}{2A_g}} \quad (10)$$

where a is the length of the beam outside the link; e, I_l, A_l, and $A_{s,l}$ are the length, moment of inertia, cross sectional, and shear areas of the link; N, h_T, b_T, and t_T are the number, height, width, and thickness of the TADAS plates; and all other parameters are as defined previously. Note that of the five terms in the denominator of (8)–(10), the second and fifth, which account for axial deformations of the bottom beam and stiffened girders could be ignored, and the fourth (accounting for
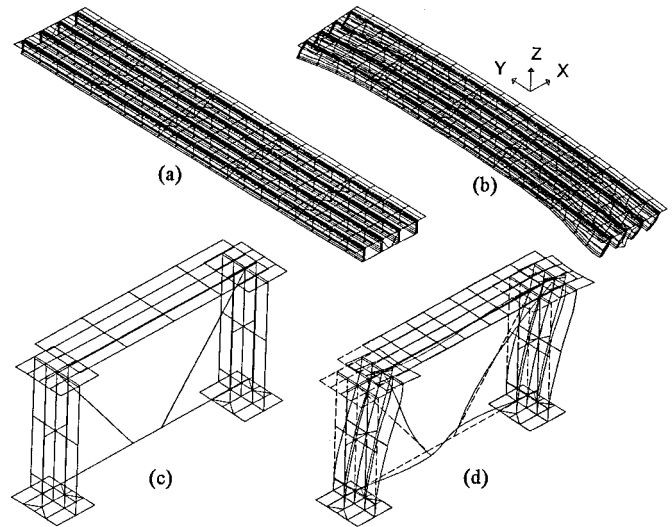
FIG. 4. Modeling of Typical Steel Slab-on-Girder Bridge Using SAP90: (a) 3D Model; (b) 3D Deformed Shape; (c) 2D Model; (d) 2D Deformed Shape (Deformed Shapes Are Greatly Magnified for Illustration Purposes)

the rotation of the bottom beam at midspan in SPS and TADAS) could have a small impact if the bottom beam was a deep and stiff beam, which is not however the case in the examples studied here.

For the above simplified model, the lateral period, T, of the steel bridge on stiff substructures considered here and retrofitted using ductile end-diaphragms is given by the following expression

$$T = 2\pi \sqrt{\frac{m^*}{K_e}} \quad (11)$$

Linear static and dynamic analyses were conducted using SAP90 (Wilson and Habibullah 1992) on 3D and 2D models (Fig. 4) of end-diaphragm structures to verify the above models of generalized mass, stiffness, lateral period, and other items for reference purposes. In all cases, comparison of results and responses at the diaphragms were satisfactory. A small difference of 5% or less was found between the lateral periods obtained by the two models for bridges of 20–60 m spans. The difference was largest for the smaller span bridges because their shear flexibility, neglected from the model expressed by (1), started to contribute more significantly to the overall deck stiffness. It is noteworthy that the fundamental lateral periods for the bridges studied here were mostly in the short period range (i.e., on the constant pseudoacceleration plateau of the design spectra), with values from 0.15 to 0.3 s.

Ductility versus Reduction Factor Strategy

Clearly, from the above description of the end-diaphragm stiffness, the flexural resistance of the girders can potentially contribute to the lateral load resistance of the ductile system, and even to its energy dissipation capability, depending on the relative rigidities of the components of this diaphragm. If the girders can be considered effectively pinned at their top and bottom, the diaphragms will exhibit an ideal bilinear hysteretic behavior [Fig. 5(a)] when subjected to severe lateral earthquake excitations, and the relationship between ductility, μ, and the force reduction factor, R, could be taken as given by the classic relationship for structures in the low period range

$$\mu = \frac{R^2 + 1}{2} \quad \text{or} \quad R = \sqrt{2\mu - 1} \quad (12a,b)$$
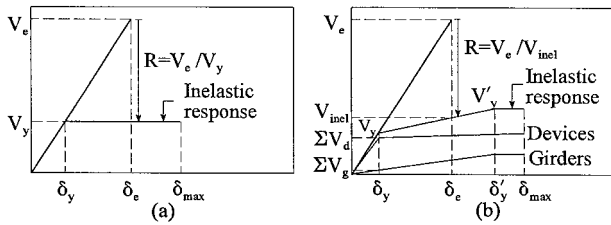
FIG. 5. Hysteretic Modeling of Seismic Resistant Systems: (a) Bilinear Model; (b) Trilinear Model

However, in the alternative situation where both the girders and ductile diaphragm element can contribute to load resistance and energy dissipation, a trilinear hysteretic model must be considered, as shown in Fig. 5(b). In that case, the relationship between ductility and the force reduction factor is somewhat more complex, and, if derived using principles of equal energy, could be demonstrated to be equal to

$$R^2 = \frac{1}{\alpha^2} \left(2U\mu - U^2(Q + 1) + Q(2U - 1) \right) \quad (13)$$

if strain hardening is neglected, where $\alpha = V_{inel}/V_y$; $U = V'_y/V_y$; and $Q = \Sigma K_{DD}/\Sigma K_g$. V_{inel} is the inelastic lateral load resistance of the entire end-diaphragm panel; V'_y and V_y are the yield strength of the stiffened girders and ductile device, respectively; and K_{DD} and K_g are as defined earlier.

In the presence of strain hardening, the above equation becomes

$$R^2 = \frac{1}{\alpha^2} \left(C_{SH}(\mu - 1 - \beta) + U(2\mu - 1 - \beta) + \beta + 1 \right) \quad (14)$$

where C_{SH} is the strain-hardening ratio; and β is as follows:

$$\beta = \frac{(U - 1)(Q + 1)}{C_{SH}Q + 1} \quad (15)$$

In all cases, since previous studies of slab-on-girder bridges (e.g., Dicleli and Bruneau 1995) and results obtained herein indicate that the steel bridges of interest in this paper have a low fundamental period of vibration in the transverse direction, the relationship between ductility and force reduction factor is based on the principle of equal energy deemed more appropriate in the low period range. On that basis, and given that lateral stiffness of the stiffened girders is usually low compared with that of the braces and energy dissipating device (leading to a modest slope along the second part of the trilinear curve), a bilinear $\mu - R$ strategy (12) was found to give good results provided an equivalent yield strength of V_{inel} and the actual device yield displacement δ_y, are used [Fig. 5(b)]. This V_{inel} is simply the actual strength of the ductile diaphragm at the lateral displacement, δ_e, that would have resulted from elastic analysis. However, in cases where the slope of the second part of the trilinear curve is relatively large and/or when V_{inel} is close to V'_y, it is recommended to use (13) or (14) instead. In all cases studied here, the equivalent bilinear strategy (12) was used.

Note that this reduction factor $(\mu - R)$ strategy was also verified using both monotonic push-over and dynamic time-history nonlinear inelastic analyses of the proposed end-diaphragm models subjected to different earthquake excitations. These analyses were carried out with the DRAIN-2DX nonlinear inelastic analysis program (Prakash et al. 1993), using plastic hinge beam column elements and truss bar elements. For SPS, in addition to a flexural element, an inelastic spring was inserted to model both elastic and inelastic shear deformations. For EBF, a similar modeling strategy was used. For TADAS systems, multiple elements were used to model stiffness variations along the height of the triangular plates. By

this modeling, trilinear behavior is implicitly considered. As consistently done in this study, equivalent springs were inserted at the connection of stub girder to slab to include the impact of slab flexibility [K^* in (4)], and an equivalent web thickness for the girder stub was used to model the actual stiffened web. Structural steel with a yield stress of 300 MPa and a strain hardening ratio of 0.01 was considered. For the dynamic analyses, tributary generalized mass lumped at the deck and Rayleigh damping of 2% were also considered, using the first and the third frequencies to calculate mass and stiffness proportional damping factors. These analyses confirmed the need to account for the nonnegligible impact of the girders' stiffness and yield strength on behavior over the displacement range of interest. The analyses also verified the effectiveness of the proposed reduction factor $(\mu - R)$ strategy.

DESIGN PROCEDURE

To achieve the desirable objective of substructure protection, ductile end-diaphragms of the type described previously must be designed to be the only structural elements to yield and dissipate energy, without ever exceeding the level of lateral load that initiates undesirable damage in the substructure. However, knowing that ductility demand and force reduction factor are intertwined, a minimum strength of the ductile diaphragms must be provided to prevent undue ductility demands on the specially detailed energy dissipating elements. Fig. 6 presents a flow chart for the proposed design procedure. In the perspective of a seismic retrofit, the necessary steps of that design procedure are:

1. Determine the following basic design parameters: superstructures mass, M; seismic acceleration coefficient, A [code-specified value (e.g., AASHTO 1994) or from site-specific data]; number of girders, n_g; number of end-diaphragms implemented at each support, n_d; girder spacing, L_s; and other geometric and descriptive characteristics of the bridge.
2. Calculate the generalized mass and stiffness, m^* and K^*, using (2a) and (2b), respectively.
3. Find the elastic seismic base shear resistance, V_e, for one end of the bridge (one-half of equivalent static force) that would be needed if fully elastic response was desirable. Typically

$$V_e = C_s \left(\frac{8Mg}{\pi^2} \right) \bigg/ 2 = C_s \frac{4Mg}{\pi^2} \approx 0.4 C_s Mg \quad (16)$$

where $C_s = 1.2AS/T^{2/3} \leq 2.5A$; g = gravity acceleration; S is the site coefficient; T is the lateral period of vibra-
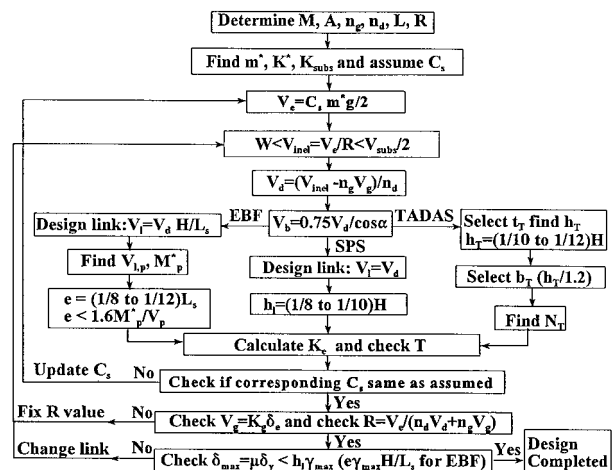
FIG. 6. Flow Chart for Proposed Design Procedure

tion; and C_s is the seismic response coefficient (AASHTO 1994). Alternatively, C_s can be taken as the pseudoacceleration, PSa, given by a smooth design spectrum (e.g., Newmark and Hall 1982).

4. Calculate $V_{\text{inel}} = V_e/R$, where V_{inel} is the inelastic lateral load resistance of the entire ductile diaphragm panel at the target reduction factor; and R is the force reduction factor mentioned earlier. Then verify that V_{inel} is less than the lateral load resistance of the substructure, with a comfortable safety factor (say 2), thus ensuring that the principal target objective is achieved. If not, this retrofit solution may not be suitable to the problem at hand, although it may be still applicable and useful to limit the extent of the required substructure retrofit work. At this time, a maximum force reduction factor of 3.75 is used here to limit ductility demands within reasonable ranges (in a load and resistance factor design context). Nonetheless, the additional constraint that $V_{\text{inel}} > W$ must also be respected, where W is the maximum expected wind force to be resisted by the diaphragms.

5. Determine the design lateral load, V_d, to be resisted by the energy dissipation device (e.g., link beam or TADAS) at the target ductility level, by

$$V_d = \frac{V_{\text{inel}} - n_g V_g}{n_d} \qquad (17)$$

where V_g = lateral load resistance of one stiffened girder. For trilinear hysteretic systems, determination of V_d would typically require an iterative calculation, as demonstrated in the examples in a later section. For expediency in a first iteration, V_g can be taken as its yield value [equal to $K_g \delta_y'$, as shown in Fig. 5(b)] or any other arbitrary value for that matter; however, its actual value at the specified transverse displacement (i.e., $K_g \delta_e$) should be considered if girders are found to remain in the elastic range in subsequent iterations. Note that in short bridges, V_g can be a dominant factor that could overwhelm the resistance contribution provided by the special ductile diaphragm elements. In that perspective, it is recommended in this procedure that the bearing stiffeners at the support of these girders be trimmed to the minimum width necessary to satisfy the strength and stability requirements. Ideally, the braced diaphragm assembly should also be 5–10 times stiffer than the girders with bearing web stiffeners (even though ductility demand tends to be larger in stiffer structures) to prevent, or at least minimize, yielding in the main girders under transverse displacements. Note that in longer bridges, particularly those with a lesser number of girders per cross section, the contribution of the girders to lateral load resistance is nearly insignificant.

6. Design all structural members and connections of the ductile diaphragm, with the exception of the seismic energy dissipation device, to be able to resist forces corresponding to $1.5V_d$, to account for potential overstrength of the ductile device due to strain hardening, strain rate effects, and higher than specified yield strength. For example, braces should be designed to resist an axial compression force, V_b, equal to

$$V_b = 1.5 \left(\frac{V_d}{2 \cos \alpha} \right) = 0.75 \frac{V_d}{\cos \alpha} \qquad (18)$$

Likewise, for the SPS and TADAS systems, the bottom beam should be designed to resist a moment equal to $1.5V_d h_l$ or $1.5V_d h_T$. Moreover, for a given SPS or TADAS device, it is also advantageous to select a flex-

urally stiff bottom beam to minimize rigid-body rotation of the energy dissipating device and thus maximize hysteretic energy at a given lateral deck displacement.

7. Design the energy dissipating device. For the devices chosen here, considerable information is available in the literature, and only the major design steps are summarized here. For example, for the link beam in an EBF end-diaphragm, the shear force V_l in the link is

$$V_l = \frac{H}{L_s} V_d \qquad (19)$$

The plastic shear capacity V_p of a wide flange beam is given by (AISC 1992)

$$V_p = 0.60F_y A_w \approx 0.55F_y t_w d_l \qquad (20)$$

where F_y is the yield stress of steel; t_w is the web thickness; d_l is the depth of the beam; and A_w is the web area. V_p must be chosen greater than, but as close as possible to V_l to meet the present objectives. The moment simultaneously applied to the link must be less than the reduced moment capacity, M_p^*, of the link yielding in shear and equal to (Malley and Popov 1983)

$$M_p^* = t_f b_f F_y (d_l - t_f) \qquad (21)$$

Because shear links are more reliable energy dissipators than flexural links (Kasai and Popov 1986; AISC 1992), shear links are favored in the current implementation and their length is therefore limited by (22)

$$e < e_{\max} = 1.6 \frac{M_p^*}{V_p} \qquad (22)$$

A link length, e, of 1/8 to 1/12 of the girder spacing, L_s, is recommended for preliminary design; the less restrictive value preferred for practical reasons (i.e., detailing constraints) in presence of closely spaced girders. Deeper link beams are also preferred as the resulting larger flexural stiffness enhances the overall stiffness of the ductile device, ensuring that its yield displacement is reached much before onset of yielding of the stiffened girders.

For a SPS, the previously mentioned procedure would be followed with the obvious exception that $V_l = V_d$ and the height of panel should be limited to one-half of the value obtained by (22), because the yielding link is only in single curvature, as opposed to double curvature for the EBF. A link height of 1/8 to 1/10 of the girder depth is recommended for preliminary design. However, for a TADAS system, replace Step 7 with Step 8.

8. Select a small plate thickness, t_T, based on available plate size. The shear strength, V_T, and the stiffness, K_T, of a TADAS device can be determined from Tsai et al. (1993)

$$V_T = \frac{N b_T t_T^2 F_y}{4 h_T} \qquad (23)$$

$$K_T = \frac{N E b_T t_T^3}{6 h_T^3} \qquad (24)$$

where N, b_T, t_T, and h_T are the number, base width, thickness, and height of the triangular steel plates, respectively. The ratio of these equations directly provides a relationship between h_T and t_T

$$h_T = \sqrt{\frac{2 E t_T V_T}{3 F_y K_T}} \qquad (25)$$

Here, $V_T = V_d$ and a h_T of $H/10$ to $H/12$ is recommended. Hence, if a reasonable estimate of the desirable K_T for the TADAS device is possible, t_T can be determined directly from h_T. In turn, b_T can be chosen knowing that triangular plates with aspect ratio, h_T/b_T, between 1 and 1.5, are better energy dissipators, based on experimental results (Tsai et al. 1993). Finally, N can then be calculated using either (23) or (24). Small adjustments to all parameters follow as N is rounded up to the nearest whole number. Incidentally, many different yet appropriate TADAS systems could be designed within these constraints.

9. Calculate the stiffness of the ductile end-diaphragm by using (8), (9), or (10) as appropriate. The lateral stiffness of the stiffened girders can be obtained from (6), (7), or other values as appropriate. Once the lateral period of the bridge, T, is computed from (11), go back to Step 3 to determine if C_s needs to be updated, and if so, repeat all previous steps until convergence.

10. For the resulting design, determine the lateral deflection of the diaphragm on a figure similar to Fig. 5(b), and calculate the base shear resistance by each of the girders and the ductile diaphragm element. At this stage, the correct value of V_g for each girder at one end of a span can be obtained based on δ_e (if $\delta_e < \delta'_y$), as shown in Fig. 5(b)

$$V_g = K_g \delta_e \leq V_{y,g} \qquad (26)$$

where $\delta_e = V_e/K_{ends}$ (K_{ends} was calculated in the previous section). Then determine the actual force reduction factor, recognizing the true trilinear behavior of the total diaphragm system, by

$$R = \frac{V_e}{V_{inel}} = \frac{V_e}{n_d V_d + n_g V_g} \qquad (27)$$

If this value is significantly different from the original target value (e.g., when larger than required members are chosen based on economic considerations), go back to Step 4 and modify the design of the device as appropriate. Note that only two or three iterations were found necessary to get acceptable final results in most cases (at least one iteration is usually required to ensure appropriateness of initial assumptions in Step 5).

11. From this final solution and actual R value, the actual displacement ductility demand can be determined from (12), (13), or (14) as appropriate, and the maximum lateral drift of the bridge at the diaphragm location, δ_{max}, is

$$\delta_{max} = \mu \delta_y \qquad (28)$$

where $\delta_y = \delta_{y,d} = V_d/K_{DD}$. Furthermore, as the maximum ductility capacity of shear links is commonly expressed in terms of the maximum link deformation angle, γ_{max} (easily obtained by dividing the maximum relative displacements of link ends by the link length), the maximum drift for the SPS and EBF diaphragms is respectively limited to

$$\delta_{max} < e \gamma_{max} \qquad (29)$$

$$\delta_{max} < \frac{eH}{L_s} \gamma_{max} \qquad (30)$$

with generally accepted γ_{max} limits of 0.09 (AISC 1992). Note that for the SPS diaphragms, the following alternative equation accounting for the rotation of bottom beam at the link connection may be more accurate when this factor has an important impact:

$$\delta_{max} < e \left(\gamma_{max} + \frac{V_d L_s (h_l + d_{bb}/2)}{12 EI_{bb}} \right) \qquad (31)$$

Should these limits be violated, modify the link's depth and length as well as the stiffness of the EBF or SPS diaphragm as necessary, and repeat the design process. Finally, a maximum drift limit of 2% of the girder height is also suggested here, at least until experimental evidence is provided to demonstrate that higher values are acceptable.

Note that the ductile energy dissipating elements should be laterally braced at their ends to prevent out-of-plane instability. These lateral supports and their connections should be designed to resist 6% of the nominal strength of the beam flange, i.e., $0.06 F_y t_f b_f$ (AISC 1992). In addition, to prevent lateral torsional buckling of beams in the SPS, EBF, and TADAS end-diaphragms, the unsupported length, L_u, of these beams shall not exceed $200 b_f / \sqrt{F_y}$, where b_f = width of beam flange in meters; and F_y = yield strength of steel in MPa.

EXAMPLES

To illustrate the proposed design procedure, a few examples are presented. In all cases, ductile diaphragms were designed considering steel with a yield stress F_y of 300 MPa, and a code-specified seismic ground acceleration of $0.3g$. The design seismic force was obtained from the AASHTO seismic provisions (AASHTO 1994), assuming a reduction factor of 3 (corresponding to a ductility capacity, μ, of 5) or 3.75 (μ, of 7.5) depending on the example. SPS, EBF, and TADAS end-diaphragms were designed for each bridge configuration and geometry considered. Table 1 presents the characteristic properties of the three slab-on-girder steel bridges considered: a simply supported 40 m span bridge, a 60-90-60 m continuous three-span bridge (diaphragms over continuous supports considered here), and a bridge having multiple simply supported 40 m spans supported by reinforced concrete bents each having four piers of 0.9 m diameter and 5 m height in one case and 0.6 m diameter and 6 m height in another case. In the latter two cases with pier cap mass of 10,000 kg, substructure stiffnesses were 146 and 16.2 kN/mm, respectively. For the 40 m span bridge examples, a single diaphragm panel was introduced between the two interior girders to obtain more practical member sizes for the key components of the ductile diaphragms.

Details of the iterative procedure are presented in Tables 2 and 3 for each example along with resulting ductilities, max-

TABLE 1. Geometric and Structural Characteristics of Steel Bridge Examples

Span (m) (1)	Deck width (m) (2)	Number of girders (3)	Girder spacing (m) (4)	Slab depth (mm) (5)	Girder size and properties (6)	I_D (m⁴) (7)	Mass (10³ kg) (8)	m^* (10³ kg) (9)	K^* (10⁸ N/m) (10)
40[a]	8	4	2	200	WWF 1,200 × 333	1.797	286	143	2.831
60-90-60 3-span	15	2	11.6	250	1,000 × 45 flanges and 5,000 × 20 Web	23.5	2,156	1,425	5.14

[a]For bridge spans on abutments or piers.

TABLE 2. Design Procedure for 40 m Simply Supported Span Bridge Examples with Target R of 3.75

Trial number (1)	V_e (kN) (2)	V_{inel} (kN) (3)	$n_g V_g$ (kN) (4)	V_d (kN) (5)	Device (6)	h_l (SPS) e (EBF) t_T (TADAS) (mm) (7)	Braces (8)	Bottom beam (9)	$n_d K_{DD}$ (N/mm) (10)	δ_y (mm) (11)	$n_g K_g$ (N/mm) (12)	K_{total} (N/mm) (13)	δ_e (mm) (14)	δ'_y (mm) (15)	$n_g V_g$ (kN) (16)	V_{inel} (kN) (17)	R (18)
(a) $T = 0.22$ s, $\mu = 7.3$, $\delta_{max} = 12.4$ mm < 24 mm $= 2\%$ H, $\gamma_{max} = 0.08 < 0.09$ rad																	
SPS 1	880	234	70	164	W150 × 14 (l_l = 230 mm)	150	2L65 × 65 × 5	W150 × 22	90,500	1.8	13,280	103,780	6.8	11	92	256	3.44
2	880	234	92	142	W150 × 14 (l_l = 200 mm)	150 St. Pl. 45 × 6	2L65 × 65 × 5	W150 × 22	86,120	1.7	13,280	99,400	7.0	11	96	238	3.7
(b) $T = 0.23$ s, $\mu = 6.5$, $\delta_{max} = 12.4$ mm < 24 mm $= 2\%$ H, $\gamma_{max} = 0.07 < 0.09$ rad																	
EBF 1	880	234	70	164	W150 × 14 (V_1 = 106 kN)	300	2L65 × 65 × 6	—	73,650	2.4	13,280	86,930	8.1	11	112	289	3.04
2	880	234	112	122	Web 120 × 4 (V_1 = 90 kN)	300 Fl. Pl. 150 × 8	2L65 × 65 × 5	Built-up section	78,770	1.9	13,280	92,050	7.6	11	104	254	3.46
(c) $T = 0.24$ s, $\mu = 7.3$, $\delta_{max} = 12.8$ mm < 24 mm $= 2\%$ H																	
TADAS 1	880	234	92	142	4Pl. 125 × 95 (b_T = 95 mm)	25	2L65 × 65 × 5	W150 × 22	55,620	2.55	13,280	68,900	10.1	11	138	280	3.14
2	880	234	138	96	4Pl. 100 × 70 (b_T = 70 mm)	25	2L65 × 65 × 5	W150 × 22	75,940	1.75	13,280	89,220	7.8	11	106	237	3.7

TABLE 3. Design Procedure for Support Diaphragms of Center 90 m Span of Three-Span Bridge Examples with Target R of 3

Trial number (1)	V_e (kN) (2)	V_{inel} (kN) (3)	$n_g V_g$ (kN) (4)	V_d (kN) (5)	Device (6)	h_l (SPS) e (EBF) t_T (TADAS) (mm) (7)	Braces (8)	Bottom beam (9)	$n_d K_{DD}$ (N/mm) (10)	δ_y (mm) (11)	$n_g K_g$ (N/mm) (12)	K_{total} (N/mm) (13)	δ_e (mm) (14)	δ'_y (mm) (15)	$n_g V_g$ (kN) (16)	V_{inel} (kN) (17)	R (18)
(a) $T = 0.50$ s < 0.33 s, $\mu = 5.3$, $\delta_{max} = 46$ mm < 100 mm $= 2\%$ H, $\gamma_{max} = 0.098$ rad																	
SPS 1	5,075	1,692	254	1,438	W360 × 179 (l_l = 580 mm)	368	2L200 × 200 × 20	W360 × 122	177,000	8.1	1,340	178,340	28.5	90	51	1,489	3.4
2	3,960	1,320	51	1,269	W360 × 179 (l_l = 520 mm)	368	2L 200 × 200 × 20	W410 × 85	139,060	8.7	1,340	140,400	28.2	90	50	1,255	3.1
(b) $T = 0.50$ s > 0.33 s, $\mu = 4.5$, $\delta_{max} = 40$ mm < 100 mm $= 2\%$ H, $\gamma_{max} = 0.093$ rad																	
EBF 1	5,075	1,692	254	1,438	W460 × 67 (V_1 = 636 kN)	1,000	2L200 × 200 × 20	—	139,860	10.3	1,340	141,200	47.9	90	86	1,539	3.3
2	3,860	1,287	64	1,223	W460 × 52 (V_1 = 564 kN)	1,000	2L200 × 200 × 20	—	144,200	9.0	1,340	145,540	26.5	90	48	1,356	2.85
(c) $T = 0.52$ s > 0.33 s, $\mu = 5$, $\delta_{max} = 51$ mm < 100 mm $= 2\%$ H																	
TADAS 1	5,075	1,692	254	1,438	9Pl. 300 × 250 (b_T = 250 mm)	50	2L200 × 200 × 20	W410 × 132	128,200	11.0	1,340	129,540	39.2	90	70	1,476	3.4
2	3,852	1,284	70	1,214	8Pl. 300 × 250 (b_T = 250 mm)	50	2L200 × 200 × 20	W410 × 132	122,730	10.2	1,340	124,070	31.0	90	55.4	1,305	3.0

imum drifts, and maximum link deformation angles (note that results identical to those in Table 2 were obtained for the bridges on piers, even though the lateral period was larger). Strain hardening was ignored for simplicity. Incidentally, design of the ductile energy dissipating elements proved easier for longer bridges with fewer girders, because the number of structural shapes having the desirable properties seemed to increase along with the strength requirements. Although flexural yielding of web stiffeners might be tolerable if it does not affect the bearing stability of the girder, it should be kept to a minimum until experimental research results can demonstrate otherwise.

Although not required by the design procedure, nonlinear inelastic static push-over analyses were conducted for the examples in Tables 2 and 3 by using DRAIN-2DX and ADINA (1995) to illustrate the trilinear behavior of the resulting ductile diaphragms and the expected extent of yielding at the design level. The DRAIN-2DX analyses were conducted on the 2D model of end-diaphragms shown in Fig. 3(a). They re-

vealed that yieldings of the device (shear yielding of link beam in SPS and EBF and flexural yielding of plates in TADAS) were obtained at a device yield strength of 142, 150, and 132 kN, when the lateral loads reached to 154, 163, and 144 kN, respectively, for SPS, EBF, and TADAS implemented in the 40 m span bridge. All other members remained elastic while the energy dissipating devices yielded. Flexural yielding in the girder web stiffeners was observed at a drift of 9 mm (corresponding to ductilities of 4–6) and a lateral load of 314, 281, and 322 kN, respectively, for SPS, EBF, and TADAS end-diaphragms. Fig. 7 illustrates the lateral load and link-beam shear versus deck displacement for SPS end-diaphragms used in the 40 and 90 m span bridge examples, respectively, pushed to a displacement ductility of approximately 7. For the 40 m single-span bridge, the lateral stiffness of the stiffened girders is not negligible compared with that of the ductile device, and the girders contribute to seismic resistance of the diaphragms as shown by the resulting trilinear curve on Fig. 7(a). By contrast, the much taller girders in the 60-90-60 m three-span

bridge do not resist a significant percentage of the lateral forces, and their flexural yielding only occurs at a very large displacement beyond the expected range of response [Figs. 7(c and d)] with a resulting bilinear load-displacement behavior over that range.

The ADINA 3D nonlinear analyses of the bridges having ductile SPS end-diaphragms and the worst case scenario of full fixity at the top and bottom of the stub girders also confirmed that the system behaved as expected. Results (Fig. 8) compared well with those obtained by the corresponding DRAIN-2DX 2D models (not shown here) up to the point of
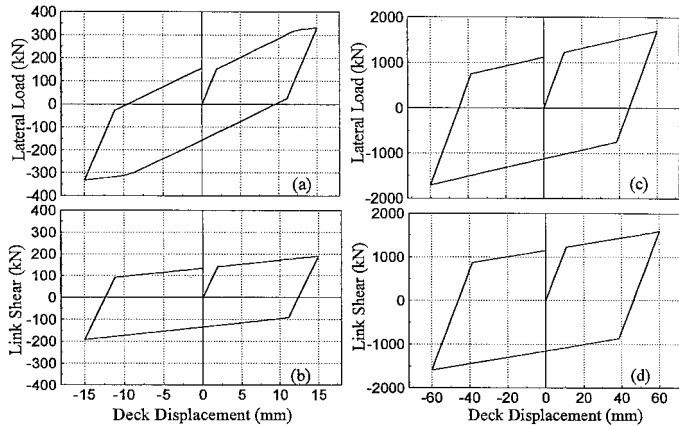
FIG. 7. Lateral Load and Link Shear Force versus Deck Displacement, Respectively, for 40 m Single-Span Bridge (a) and (b) and in Tensor Support of Three-Span Bridge (c) and (d), having Side Span of 60 m and Center Span of 90 m, with SPS Diaphragms (Push-Over Analyses)
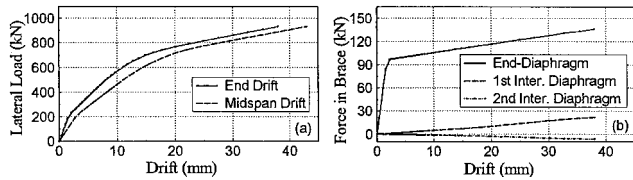
FIG. 8. Inelastic 3D Analysis Results for 40 m Span Bridge Having SPS End-Diaphragms by ADINA (Web Stiffeners only at Supports): (a) Lateral Load versus End and Center Drifts; (b) Axial Forces in Braces versus End Drift

shear yielding of the SPS, δ_y. However, the 3D analyses indicated that the stiffened girders contribute about 15% more to the lateral load resistance at a drift of δ_{max}. Interestingly, as shown in Fig. 8(b), intermediate diaphragms do not contribute significantly to the lateral load resistance of the retrofitted bridges. This is consistent with findings reported for non-retrofitted slab-on-girder bridges as previously demonstrated by the writers (Zahrai and Bruneau 1998).

Inelastic Dynamic Time-History Analysis

To validate the ductile diaphragm seismic retrofit concept, the 2D structural model was also analyzed using nonlinear inelastic time history analyses using the DRAIN-2DX program and considering five different earthquake excitations scaled to $0.4g$ and applied transversely to the span direction. The 1940 El-Centro S00E, 1966 Parkfield N65E, 1971 Pacoima Dam S16E, 1988 Saguenay (St-Ferreol, longitudinal component), and 1989 Loma Prieta (Corralitos 37.037N 121.883W), were considered. Rayleigh damping was used with 2% ($\xi = 0.02$) damping assigned to the first and third periods (0.24 and 0.14 s for the simple span bridges).

Table 4 represents inelastic analysis results for the 40 m span bridge examples using final member sizes for the three end-diaphragms (SPS, EBF, and TADAS) obtained following the proposed design procedure. Resulting inelastic time-history analyses (deck displacements and link rotations) for the example bridge models with SPS end-diaphragms subjected to the 1940 El-Centro earthquake are also presented in Fig. 9 for illustration purposes (note different scales for y-axes). As shown in Figs. 9(e and f) and Table 4 for the average of all earthquakes considered, maximum ductilities and drift results remain within the expected range for bridges on stiff pier bents. However, excessive ductility demands were obtained for the bridges on more flexible piers [Figs. 9(g and h)]. In that later case, the generalized mass and stiffness of the proposed design procedure, developed for bridges on stiff piers, is significantly in error. Further studies are needed to improve the procedure, as well as to quantify the limit of applicability of the ductile diaphragm retrofit technique in terms of a ratio of superstructure-to-substructure stiffnesses.

TABLE 4. Nonlinear Inelastic Response of 40 m Span Bridges with Ductile Diaphragms Using Strain-Hardening Ratio of 0.01 (Relative Displacements Are Reported)

| | | TIME-HISTORY ANALYSIS | | | | | | | | | | | | |
| | | El-Centro | | Parkfield | | Pacoima Dam | | Saguenay | | Loma Prieta | | Average | | |
Case (1)	Period (s) (2)	δ_{max} (mm) (3)	γ_{max} (4)	δ_{max} (mm) (5)	γ_{max} (6)	δ_{max} (mm) (7)	γ_{max} (8)	δ_{max} (mm) (9)	γ_{max} (10)	δ_{max} (mm) (11)	γ_{max} (12)	δ_{max} (mm) (13)	μ_{max} (14)	γ_{max} (15)
SPS	0.236	12.0	0.060	19.5	0.106	8.1	0.038	15.6	0.081	8.9	0.042	12.8	6.7	0.065
EBF	0.238	10.1	0.039	14.6	0.059	7.9	0.030	11.4	0.045	7.8	0.030	10.4	5.0	0.041
TADAS	0.245	12.9	—	23.1	—	8.7	—	19.0	—	11.2	—	15.0	7.5	—
SPS[a]	0.274	11.1 (2.1)	0.055	22.6 (2.6)	0.123	8.4 (1.8)	0.039	18.5 (2.5)	0.098	12.1 (2.2)	0.060	14.5	7.6	0.075
EBF[c]	0.275	9.0 (2.1)	0.034	18.3 (2.7)	0.077	7.4 (1.9)	0.027	15.2 (2.6)	0.063	7.5 (1.9)	0.027	11.5	5.5	0.046
TADAS[a]	0.35	8.9 (15.2)	—	20.2 (17.8)	—	8.4 (14.9)	—	15.5 (17.4)	—	7.2 (13.9)	—	12.0	6.0	—
SPS[b]	0.48	31.1 (26.6)	0.171	38.1 (27.7)	0.210	8.6 (16.6)	0.040	31.1 (26.2)	0.173	26.8 (24.7)	0.148	27.1	14.2	0.148
EBF[b]	0.48	28.5 (28.1)	0.128	36.8 (29.5)	0.158	8.9 (18.3)	0.033	24.5 (26.9)	0.111	10 (19.4)	0.039	21.7	10.4	0.094
TADAS[b]	0.86	23 (155)	—	4.7 (100)	—	2.7 (79)	—	3.5 (95)	—	27 (160)	—	12.2	6.1	—

Note: Numbers in parentheses refer to the drifts of the pier caps.
[a]Multispan simply supported 40 m span bridge on concrete bents, each having four 900 mm diameter columns (5 m tall).
[b]Multispan simply supported 40 m span bridge on concrete bents, each having four 600 mm diameter columns (6 m tall).
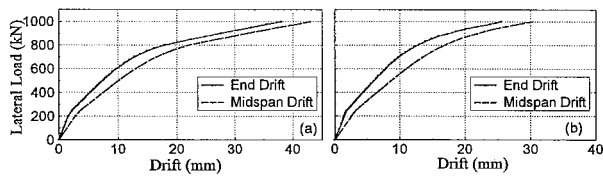
FIG. 9. Inelastic Time-History Analyses for 40 m and 90 m Span Bridges Subjected to El-Centro Earthquake Scaled to 0.4*g* (for First 10 sec): (a) Deck Displacement; and (b) Link Rotation for 90 m Span Bridge; (c) Deck Displacement; and (d) Link Rotation for 40 m Span Bridge; (e) and (f) Same for Bridge on Stiff Piers; (g) and (h) Same for Bridge on Flexible Piers
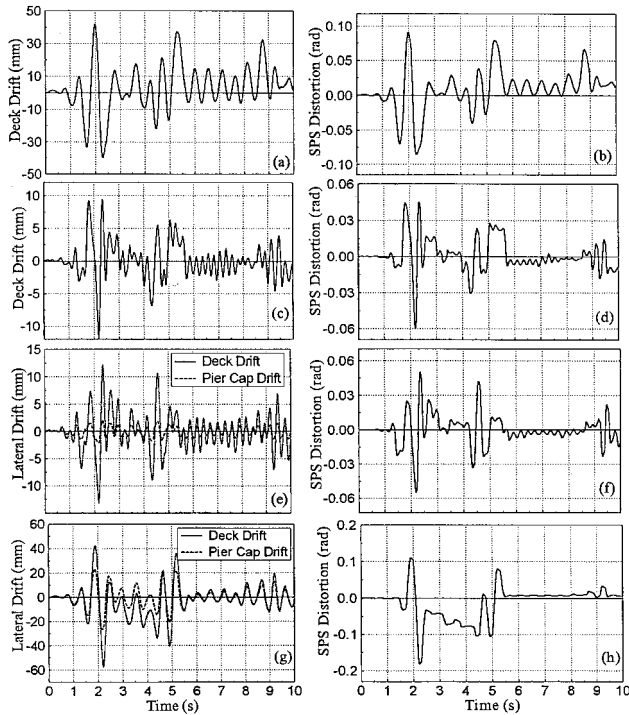
FIG. 10. Impact of Intermediate Web Stiffeners on Proposed Design Procedure
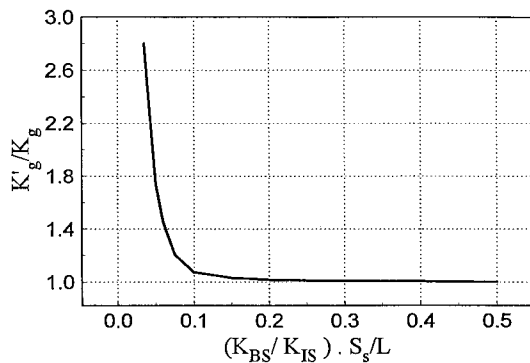
FIG. 11. Lateral Load versus End and Center Drifts Based on Inelastic 3D Analysis Results by ADINA, for 40 m Span Bridge Having SPS End-Diaphragms and Double-Sided 100 × 10 mm Web Stiffeners at: (a) Every 4 m; (b) Every 2 m

Impact of Intermediate Web Stiffeners

In the proposed design procedure and above examples the girders were assumed to have no intermediate web stiffeners. In the presence of such stiffeners, the lateral stiffness, K_g, of the girders used in the above procedure should be modified. This can be done by using an equivalent lateral stiffness, K_g', instead of K_g in (5). No closed-form solution is provided for K_g' at this time, but Fig. 10 shows the nondimensional relationship between K_g'/K_g and $(K_{BS}/K_{IS})S_s/L$, where S_s is spacing

of intermediate web stiffeners, L is bridge span, and K_{BS} and K_{IS} are, respectively, the lateral stiffnesses of the bearing and intermediate web stiffeners with respect to the girder longitudinal axis. Fig. 10 was obtained by running ADINA for bridges of various spans having different intermediate web stiffener's stiffnesses and spacings. Generally, the impact of intermediate web stiffeners on K_g can be ignored, unless large stiffeners are used at small intervals. For example, if intermediate stiffeners identical in size to the bearing web stiffeners (i.e., $K_{BS} = K_{IS}$) are used at an interval of 0.1L, K_g' would be only 6% greater than K_g. Fig. 11 compares the inelastic analysis results for the same 40 m span bridge of Fig. 8, but having 100 × 10 mm web stiffeners at every 4 m and 2 m. In general, the farther transverse web stiffeners are from bridge ends the smaller is their contribution to the lateral load resistance.

CONCLUSIONS

This paper demonstrates that it is possible, in some instances, to seismically retrofit slab-on-girder steel bridges by replacing their existing end-diaphragms with new ductile diaphragms incorporating stable seismic energy dissipation devices. By means of capacity design principle, these devices act as structural fuses and can be calibrated to yield before the strength of the substructure is reached, thus protecting that substructure from undesirable damage.

Example retrofits are accomplished using a simple design procedure developed for hand calculation based on a trilinear load-displacement relationship and a strength-versus-ductility relationship based on equal energy concepts. Nonlinear inelastic analyses suggest that the resulting designs will exhibit an appropriate ultimate cyclic seismic behavior. More effective retrofits using ductile end-diaphragms are obtained for longer bridges having a smaller number of girders. It was also found that the impact of intermediate diaphragms and web stiffeners is minor unless these are closely spaced along the girders near to the supports.

However, although the concept is promising and appears satisfactory for spans supported on stiff substructures based on the limited analyses reported here, more research is needed before common implementation is possible. In particular, large scale experimental verification of the concept and expected behavior is desirable, as well as parametric studies to investigate the range of substructure stiffnesses for which this retrofit strategy can be effective.

ACKNOWLEDGMENTS

APPENDIX. REFERENCES

AASHTO LRFD bridge design specification. (1994). American Association of State Highway and Transportation Officials, Washington, D.C.

ADINA R & D, Inc. (1995). "Automatic dynamic incremental nonlinear analysis." *ADINA software and documentations*, ADINA, Watertown, Mass.

American Institute of Steel Construction (AISC). (1992). *Seismic provisions for structural steel buildings.* AISC, Chicago, Ill.

Astaneh-Asl, A. (1993). "Seismic retrofit concepts for the East Bay Crossing of the San Francisco-Oakland Bay bridge." *Proc., 1st U.S. Seminar on Seismic Evaluation and Retrofit of Steel Bridges*, San Francisco, Calif.

Astaneh-Asl, A., Bolt, B., Mcmullin, K. M., Donikian, R. R., Modjtahedi, D., and Cho, S. W. (1994). "Seismic performance of steel bridges during the 1994 Northridge earthquake." *UCB Rep. CE-STEEL 94/01*, University of California, Berkeley, Calif.

"Bridge seismic retrofit study for Southwest Admiral-South bridge." (1993). *Final Rep.*, Seattle Engineering Department, Seattle, Wash.

Bruneau, M., Wilson, J. W., and Tremblay, R. (1996). "Performance of steel bridges during the 1995 Hyogoken-Nanbu (Kobe, Japan) earthquake." *Can. J. Civ. Engrg.*, 23(3), 678–713.

Buckle, I. G., Mayes, R. L., and Button, M. R. (1986). "Seismic design and retrofit manual for highway bridges." *Computech Engrg. Services*, published also as *Rep. FHWA-IP-87-6*, U.S. Department of Transportation, Federal Highway Administration, Washington, D.C.

Degenkolb, O. H. (1978). "Retrofitting bridges to increase seismic resistance." *J. Tech. Councils*, ASCE, 104(1), 13–20.

Dicleli, M., and Bruneau, M. (1995). "Seismic performance of single-span simply-supported and continuous slab-on-girder steel highway bridges." *J. Struct. Engrg.*, ASCE, 121(10), 1497–1506.

Fehling, E., Pauli, W., and Bouwkamp, J. G. (1992). "Use of vertical shear-links in eccentrically braced frames." *Proc., 10th World Conf. on Earthquake Engrg.*, Vol. 9, Madrid, 4475–4479.

Kasai, K., and Popov, E. P. (1986). "Cyclic web buckling control for shear link beams." *J. Struct. Engrg.*, ASCE, 112(3), 505–523.

Malley, J. O., and Popov, E. P. (1983). "Design considerations for shear links in eccentrically braced frames." *EERC Rep. 83-24*, University of California, Berkeley, Calif.

Mander, J. B., Kim, D.-K., Chen, S. S., and Premus, G. J. (1996). "Response of steel bridge bearings to reversed cyclic loading." *Tech. Rep. NCEER-96-0014*, National Center for Earthquake Engineering Branch, Buffalo, N.Y.

Mayes, R. L., Buckle, I. G., Kelly, T. E., and Jones, L. R. (1992). "AASHTO seismic isolation design requirements for highway bridges." *J. Struct. Engrg.*, ASCE, 118(1), 284–304.

Mayes, R. L., Jones, D. M., Knight, R. P., Choudhury, D., and Crooks, R. S. (1994). "Seismically isolated bridges come of age." *Proc., 4th Int. Conf. on Short and Medium Span Bridges*, Canadian Society of Civil Engineering, Montreal, 1095–1106.

Nakashima, M. (1995). "Strain-hardening behavior of shear panels made of low-yield steel. I: Test." *J. Struct. Engrg.*, ASCE, 121(12), 1742–1749.

Newmark, N. M., and Hall, W. J. (1982). *Earthquake spectra and design.* Earthquake Engineering Research Institute, Oakland, Calif.

Prakash, V., Powell, G. H., and Campbell, C. (1993). "DRAIN-2DX base program description and user guide." *Rep. No. UCB/SEMM 93/17*, University of California, Berkeley, Calif.

Priestley, M. J. N., Seible, F., and Chai, Y. H. (1992). "Seismic retrofit of bridge columns using steel jackets." *Proc., 10th World Conf. on Earthquake Engrg.*, Vol. 9, Balkema, Rotterdam, The Netherlands, 5285–5290.

Roberts, J. E. (1992). "Sharing California's seismic lessons." *Modern Steel Constr.*, 7, 32–37.

"Seismic Retrofitting Guidelines for Highway Bridges." (1983). *Rep. ATC-6-2*, Applied Technology Council, Palo Alto, Calif.

Shirolé, A. M., and Malik, A. H. (1993). "Seismic retrofitting of bridges in New York State." *Proc., Symp. on Practical Solutions for Bridge Strengthening and Rehabilitation*, Iowa State University, Ames, Iowa, 123–131.

Tsai, K. C., Chen, H. W., Hong, C. P., and Su, Y. F. (1993). "Design of steel triangular plate energy absorbers for seismic-resistance construction." *Earthquake Spectra*, 9(3), 505–528.

Wilson, E. L., and Habibullah, A. (1992). "SAP90 computer software for structural and earthquake engineering." *Computers and Structures Inc.*, Berkeley, Calif.

Zahrai, S. M., and Bruneau, M. (1998). "Impact of diaphragm on seismic response of straight slab-on-girder steel bridges." *J. Struct. Engrg.*, ASCE, 124(8), 938–947.